Journal of Robotics and Control (JRC)
Volume 5, Issue 6, 2024
ISSN: 2715-5072, DOI: 10.18196/jrc.v5i6.23577 

# Cooperative Formation and Obstacle Avoidance Control for Multi-UAV Based on Guidance Route and Artificial Potential Field

Mochammad Sahal [1*], Vincentius Charles Maynad [2], Yusuf Bilfaqih [3]
[1, 2, 3] Department of Electrical Engineering, Institut Teknologi Sepuluh Nopember, Surabaya, Indonesia
Email: [1] sahal@its.ac.id, [2] vincentiuscm@gmail.com, [3] bilfaqih@ee.its.ac.id
*Corresponding Author

***Abstract*—Research on cooperative control of multi-UAV systems has gained significant attention in the flight control field, with a particular focus on formation control and obstacle avoidance due to their complexity and importance. This paper introduces an approach to a group of quadcopter control by integrating fuzzy controller, guidance route, and Artificial Potential Field (APF) methods. The quadcopter dynamic model, featuring six degrees of freedom, is controlled using a fuzzy state feedback controller in its inner loop. From the outer loop, the formation-making is guided by an easy-to-use and versatile guidance route approach while obstacle avoidance is tackled using the optimal APF method. There are two avoidance strategies that can be compared and analyzed, called "total avoidance" and "minimal avoidance", both individually and as a "combined" strategy. Simulations in various environments with different obstacle sizes show that all control algorithms can accomplish the tasks effectively. Both strategies have their own strength in terms of path length and formation maintenance. A formation performance index, which is calculated based on the difference between the desired position and the actual position of each quadcopter, is used to quantify the effectiveness of the method. A smaller value means better formation maintenance. The total avoidance strategy achieved an average index of 0.8000 and the minimal avoidance strategy reached 1.2227. These metrics highlight the trade-offs of each strategy in maintaining optimal formation. These findings offer valuable insights for the development of more robust multi-UAV systems, with potential applications in autonomous delivery services, surveillance, and environmental monitoring.**

***Keywords*—Artificial Potential Field; Fuzzy Controller; Guidance Route; Multi-UAV; Total and Minimum Avoidance Strategies.**

## I. INTRODUCTION

An Unmanned Aerial Vehicle, commonly referred to as UAV, is an aerial vehicle utilizing aerodynamic forces to produce lift and achieve the remarkable capability of autonomous flight with no pilot on board [1]. It may contain sensors, communication devices, as well as other payload devices [2]. Among the vast UAV configurations in use today, the quadcopter has emerged as a preeminent choice [3]. A quadcopter is a rotary wing type UAV using a propeller in the process of flight [4]. When viewed from the system, a quadcopter has six degrees of freedom [5]–[7] three degrees for translational movement about the X, Y, and Z axes and three others for rotational motion with respect to the Euler angles roll $\phi$, pitch $\theta$, and yaw $\psi$.

In recent years, multi-UAV has become a hot research topic in the field of flight control [8]–[16]. Among the various facets of this evolving discipline, the subject of formation control is an important theme to study [17], holding profound significance in both military and civilian sectors [18]–[23]. With the increasing complexity of modern battlefields and task requirements, it has become very urgent to complete a specific task with multi-UAV [24]. Notably, this imperative extends beyond the realm of aerial vehicles, encompassing a spectrum that spans from multi-robot systems [25]–[27], underwater vehicles [20], [28]–[30], up to spacecraft [31]–[33]. In this context, the main purpose of formation control is devising a control strategy that not only guides all agents toward the desired formation but also upholds stringent standards of tracking precision and attitude synchronization [34].

A multitude of methodologies have been put forth to tackle the intricate task of formation control, each offering its own unique approach and advantage. These encompass the leader-follower paradigm [35]–[37], the concept of virtual structure [38]–[40], consensus-driven techniques [41]–[43], and behavior-based strategies [44]. Among them, the leader-follower approach has garnered substantial attention within contemporary literature.

The leader-follower methodology hinges upon a designated leader within a group, an agent vested with knowledge of the trajectory that should be followed or the target that must be pursued. The remaining agents are considered followers and move based on the leader whose information is obtained through internal communications. The followers are directed to form and maintain formation along with the leader using a specific control protocol. The leader-follower method has been discussed in the formation control of air vehicles [45], mobile robot [46], and surface vehicles [47]. However, it is worth noting that these works are still limited to a two-dimensional operational space, representing a limitation in the field's scope.

The methods for formation control can be broadly classified into 3 categories [48], [49]. The first of these categories is known as position-based formation control (PFC) [50]–[52]. In this technique, the focal point of control for each agent centers on the disparity between its present position and the desired position within the formation. This method exhibits suitability for applications involving low-

speed vehicles with omnidirectional capabilities. One of the latest developments in the guidance method introduced by [53], aims to achieve coordinated formation control and is subsequently tested on fixed-wing UAVs. The second classification is displacement-based formation control (DFC) [54]. Within DFC, each agent directs its attention towards its own displacement concerning other agents and takes proactive measurements to govern the divergence of its displacement from the intended trajectory. The reference can be seen at [54]. A notable limitation of DFC is its reliance on real-time knowledge of the relative positions of neighboring agents. The third class is called Distance-Based formation control [55]. This variant operates by establishing and maintaining specific spacing between agents to attain a formation characterized by predefined inter-agent distances. Unfortunately, precision can be challenging to achieve, and existing research only uses the single-integrator model.

Furthermore, the application of formation control within complex environments has also been studied. The examples in this scenario involve obstacle avoidance and constraints related to communication. Obstacle avoidance of multi-UAV systems presents distinctive challenges when compared to single UAV operations. Formation obstacle avoidance refers to the formation control behavior to avoid obstacles and finally reach the target point [56]. Several prevalent methodologies have been employed for this purpose, including a geometry-based approach [57], [58], consensus-based [59], [60], potential-based technique [61], [62], and even more contemporary methods such as the optimization method [63] and heuristic algorithm [64].

One noteworthy algorithm for obstacle avoidance is known as Artificial Potential Field (APF) [65]–[69] which operates by generating an artificial force field around both obstacles and the target destination. APF relies on sensor data collected by quadcopters to facilitate obstacle avoidance [70]. However, the approach employed by APF remains constant irrespective of the type of obstacles encountered, potentially leading the formation to easily divided to avoid them, as seen in [56], [71], [72]. Meanwhile, we want the formation to be maintained as much as possible during the process. Given the diversity of the formation and obstacle sizes, a more adaptive method to enhance the effectiveness of formation control in such a situation is needed.

From the literature review above, most of the works still use linear models or integrators to describe the dynamics of the agents. Sometimes it is also limited to a two-dimensional scope. This study addresses these limitations by proposing a nonlinear, adaptive approach that enhances formation stability and obstacle avoidance in complex environments. In this paper, a novel cooperative formation obstacle avoidance control algorithm that integrates guidance routes with an optimal APF method is introduced, addressing the limitations of current techniques by adapting to varying obstacle sizes and formation dynamics. Guidance routes are used to carry out coordinate-based formation control that is accurate but easy to implement. Meanwhile, optimal APF considers the final goal in the avoidance algorithm to produce smoother avoidance.

The main contributions of this paper are as follows:

1) Proposing a cooperative formation obstacle avoidance control algorithm based on guidance route and optimal APF for a nonlinear six degrees of freedom quadcopter model.
2) Develop three novel strategies for obstacle avoidance. They are "total avoidance", which focuses on the optimal range of avoidance based on the formation size, "minimal avoidance", tailored to minimize deviations while navigating around small obstacles, and "combined" approach. These strategies serve to demonstrate the effectiveness and flexibility of the proposed method.

The remainder of this paper is organized as follows: Section II presents the proposed formation and obstacle avoidance control methods. Section III provides simulation results and discussion. Finally, Section IV concludes the study and outlines directions for future research.

## II. METHOD

In this section, we describe the quadcopter model as well as the control method that we used to control the copter. We propose a new approach to formation obstacle avoidance control by combining the guidance route and the optimal APF method. Simply put, the guidance route will cover the formation control while APF makes sure the formation is always safe from any obstacles. We also modified the obstacle avoidance strategy and produced two variations in the process. They are called "total avoidance" and "minimal avoidance". The total avoidance strategy forces the formation to take a turn as big as the formation shape size. With this approach, the formation will never be divided because they always avoid the obstacle together. On the other hand, minimal avoidance is only willing to avoid the obstacle with the smallest turn possible. Both strategies have their own advantages and disadvantages that will be discussed later in the fourth section. Then, we combine them as a "combined" strategy to exploit the advantages of each strategy.

### *A. Quadcopter Model*

The type of quadcopter utilized is Quanser Qdrone as shown in Fig. 1. This drone has been widely used for outdoor research, such as [73]–[80]. The frame size is 40 cm × 40 cm × 15 cm, it is durable and lightweight.

The dynamic model of the quadcopter is derived based on its motion on the earth frame (*E*-frame) and body frame (*B*-frame). The translational motion model, which consists of position $[X \;\; Y \;\; Z]^T$ and velocity $[\dot{X} \;\; \dot{Y} \;\; \dot{Z}]^T$, is formulated from the earth frame. Meanwhile, rotational motion, namely roll $\phi$, pitch $\theta$, yaw $\psi$, and their respective speeds use the body frame because it is related to the quadcopter's movement toward itself.

We describe the motion of the quadcopter using the degrees of freedom model [81], as follows:

$$\ddot{X} = (\sin\phi \sin\psi + \cos\phi \sin\theta \cos\psi)\frac{U_1}{m} \quad (1)$$

$$\ddot{Y} = (-\sin\phi\cos\psi + \cos\phi\sin\theta\sin\psi)\frac{U_1}{m} \quad (2)$$

$$\ddot{Z} = -g + (\cos\phi\cos\theta)\frac{U_1}{m} \quad (3)$$

$$\dot{p} = \frac{J_{yy} - J_{zz}}{J_{xx}}qr + \frac{U_2 l}{J_{xx}} \quad (4)$$

$$\dot{q} = \frac{J_{zz} - J_{xx}}{J_{yy}}pr + \frac{U_3 l}{J_{yy}} \quad (5)$$

$$\dot{r} = \frac{J_{xx} - J_{yy}}{J_{zz}}pq + \frac{U_4 d}{J_{zz}} \quad (6)$$

where $\ddot{X}$, $\ddot{Y}$, and $\ddot{Z}$ are quadcopter's acceleration on the three Cartesian axes. $p$, $q$, and $r$ are the roll ($\phi$) speed, pitch ($\theta$) speed, and yaw ($\psi$) speed, respectively. While $U_1$, $U_2$, $U_3$, and $U_4$ are the forces acting on the thrust, roll, pitch, and yaw. The quadcopter parameters can be seen in Table I.

Fig. 1. Quanser Qdrone [82]

TABLE I. QUADCOPTER PARAMETERS

| Symbol | Parameter (unit) | Value |
|---|---|---|
| $m$ | Mass ($kg$) | 1 |
| $g$ | Gravitational acceleration $\left(\frac{m}{s^2}\right)$ | 9.81 |
| $J_{xx}$ | Moment of inertia about the X axis ($kg.m^2$) | 0.03 |
| $J_{yy}$ | Moment of inertia about the Y axis ($kg.m^2$) | 0.03 |
| $J_{zz}$ | Moment of inertia about the Z axis ($kg.m^2$) | 0.04 |
| $l$ | The distance of the motor from the center of the mass ($m$) | 0.2 |
| $d$ | Drag constant ($N$) | $3.13 \times 10^{-5}$ |

TABLE II. STATE FEEDBACK CONTROLLER PARAMETERS

| Parameter | Value | Parameter | Value |
|---|---|---|---|
| $K_1$ | 16 | $L_1$ | 9 |
| $K_2$ | 100 | $L_2$ | 21 |
| $K_3$ | 100 | $L_3$ | 21 |
| $K_4$ | 0.09 | $L_4$ | 0.61 |

## B. Quadcopter Control

The quadcopter control scheme used as a tracking controller is divided into two parts, position controller as the outer loop and attitude controller as the inner loop which can be seen in Fig. 2. The state feedback controller is used to control altitude ($Z$) and heading ($\psi$). Meanwhile, a combination of state feedback controller and Sugeno-type fuzzy logic controller is used to control positions $X$, $Y$ and attitudes $\phi$, $\theta$. This control scheme is used for all quadcopters uniformly.

The input of the position control is the reference position $[X_{ref}(t) \quad Y_{ref}(t) \quad Z_{ref}(t)]^T$ and the quadcopter's actual position $[X(t) \quad Y(t) \quad Z(t)]^T$. Then, the controller outputs are $U_1$, $s_{7_{ref}}(t)$, and $s_{8_{ref}}(t)$. Next, $s_{7_{ref}}(t)$, $s_{8_{ref}}(t)$, and quadcopter angular position $[\phi(t) \quad \theta(t) \quad \psi(t)]^T$ would become inputs for attitude control which produces $U_2$, $U_3$, and $U_4$. $s_7$ and $s_8$ are variables that will be controlled by the state feedback controller to produce $U_2$ and $U_3$.

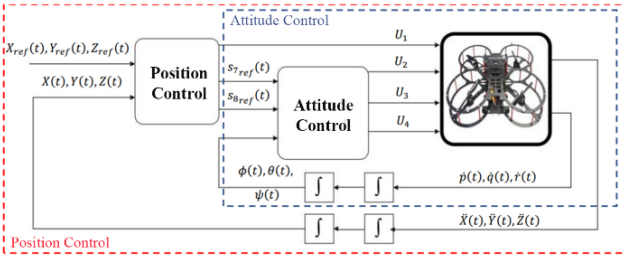


Fig. 2. Block diagram of quadcopter flight control.

*1) Position control:* To control the X and Y positions, a fuzzy controller is utilized. The controller has 2 inputs i.e. the distance and the velocity. It is assumed that the distance is the difference between the current ($X$ and $Y$) position of the quadcopter to the reference position. If the distance is greater than 25 meters, it will enter the "far" category. For the "middle" category, if the distance is between 6 and 25 meters. Distance smaller than 6 meters will enter the "close" category. Velocity is the difference between the current quadcopter velocity ($\dot{X}$ and $\dot{Y}$) and the reference velocity. If the velocity is greater than $4\frac{m}{s}$ then it is included in the "fast" category. As for the "slow" category, if the velocity is less than $4\frac{m}{s}$.

Consequently, the desired controller outputs, $s_{7_{ref}}(t)$ and $s_{8_{ref}}(t)$, become input for the $\phi$ and $\theta$ controller. The output value is limited to $-0.5 < ref < 0.5$, assuming the maximum tilt of the quadcopter is 30º. The rule base that applies is summarized in Table III. The rule base values are obtained from basic knowledge about the system and tested through a trial and error process similar to the method for obtaining state feedback controller parameters.

TABLE III. FUZZY CONTROLLER RULE BASE

| Distance | Velocity | $ref$ |
|---|---|---|
| Far | Fast or slow | 0.5 |
| Middle | Fast | 0.3 |
| Close | Fast | - 0.5 |
| Close | Slow | 0 |

For altitude control, (3) is modified by adding drag force to the equation, thus

$$\ddot{Z} = -g + (\cos\theta\cos\phi)\frac{U_1}{m} - d.\dot{Z} \quad (7)$$

Where

$$U_1 = \frac{m}{\cos\phi\cos\theta}\left(g + K(Z_{ref} - Z) + L(\dot{Z}_{ref} - \dot{Z}) + \ddot{Z}_{ref} + d.\dot{Z}\right) \quad (8)$$

By substituting (8) to (7), the state equation becomes

$$\ddot{Z} = K_1(Z_{ref} - Z) + L_1(\dot{Z}_{ref} - \dot{Z}) + \ddot{Z}_{ref} \quad (9)$$

*2) Attitude control:* The copter heading is controlled by a state feedback control so that the value of $\psi \to 0$ using

$$U_4 = \frac{J_{zz}}{D}\left(-K_4\psi - L_4\dot{\psi}\right) \quad (10)$$

If (10) is substituted to (6), the equation becomes

$$\dot{r} = \frac{J_{xx} - J_{yy}}{J_{zz}} pq - K_4\psi - L_4\dot{\psi} \quad (11)$$

Since the value of $J_{xx} = J_{yy}$, (11) can be simplified to

$$\dot{r} = -K_4\psi - L_4\dot{\psi} \quad (12)$$

Due to $\psi$ is controlled to 0, (1) can also be simplified to

$$\ddot{X} = (\sin\phi \sin 0 + \cos\phi \sin\theta \cos 0)\frac{U_1}{m} = (s_7)\frac{U_1}{m} \quad (13)$$

where $s_7 = cos\,\phi\, sin\,\theta$. $s_7$ can be seen as a controlled variable to obtain the desired roll value. It is assumed that its derivative is equal to $p$, $\dot{s}_7 = p$, and

$$\ddot{s_7} \approx \dot{p} = \frac{J_{yy} - J_{zz}}{J_{xx}} qr + \frac{U_2 l}{J_{xx}} \quad (14)$$

So

$$U_2 = \frac{J_{xx}}{l}(K_2 s_{7_{ref}} - K_2 s_7 - L_2 \dot{s}_{7_{ref}} - L_2 \dot{s}_7 + \ddot{s}_{7_{ref}}) \quad (15)$$

If (15) is substituted to (4), the equation becomes

$$\ddot{s_7} \approx \dot{p} = \frac{J_{yy} - J_{zz}}{J_{xx}} qr + K_2 s_{7_{ref}} - K_2 s_7 - L_2 \dot{s}_{7_{ref}} - L_2 \dot{s}_7 + \ddot{s}_{7_{ref}} \quad (16)$$

Based on Table I, the difference between $J_{yy}$ and $J_{yy}$ is very small so it is considered to be 0, hence

$$\ddot{s_7} \approx \dot{p} = K_2 s_{7_{ref}} - K_2 s_7 - L_2 \dot{s}_{7_{ref}} - L_2 \dot{s}_7 + \ddot{s}_{7_{ref}} \quad (17)$$

By using the same method, some equations regarding $\ddot{Y}$, $U_3$, and $\ddot{s_8}$ can be obtained, such as

$$\begin{aligned}\ddot{Y} &= (-\sin\phi \cos 0 + \cos\phi \sin\theta \sin 0)\frac{U_1}{m} \\ &= -(s_8)\frac{U_1}{m}\ddot{s_7} \approx \dot{p} \\ &= K_2 s_{7_{ref}} - K_2 s_7 - L_2 \dot{s}_{7_{ref}} \\ &\quad - L_2 \dot{s}_7 + \ddot{s}_{7_{ref}}\end{aligned} \quad (18)$$

where $s_8 = sin\,\phi$ and $\dot{s}_8 = q$,

$$U_3 = \frac{J_{yy}}{l}(K_3 s_{8_{ref}} - K_3 s_8 - L_3 \dot{s}_{8_{ref}} - L_3 \dot{s}_8 + \ddot{s}_{8_{ref}}) \quad (19)$$

Also

$$\ddot{s_8} \approx \dot{q} = K_3 s_{8_{ref}} - K_3 s_8 - L_3 \dot{s}_{8_{ref}} - L_3 \dot{s}_8 + \ddot{s}_{8_{ref}} \quad (20)$$

Attitude control $\phi$ and $\theta$ using state feedback requires reference input ($s_{7_{ref}}$, $\dot{s}_{7_{ref}}$, $\ddot{s}_{7_{ref}}$, $s_{8_{ref}}$, $\dot{s}_{8_{ref}}$, $\ddot{s}_{8_{ref}}$) in order to produce the desired output. These reference values are the output of the fuzzy logic controller. The schematic can be seen in Fig. 3. The value of the state feedback controller parameter is obtained through a trial-and-error process by providing waypoints. When the quadcopter succeeds in reaching all the specified targets, the parameters can be used. The parameter values used are written in Table II.

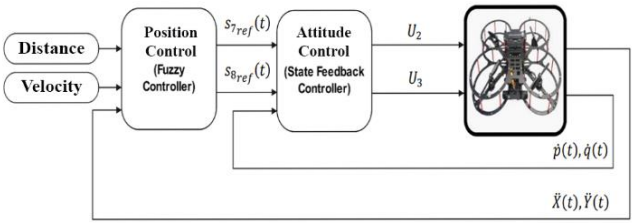


Fig. 3. Block diagram of roll $\phi$ and pitch $\theta$ control

### C. Formation Control Design

The desired formation is a V-shape formation. Fig. 4 and Table IV describe the V shape more clearly. Fig. 4 shows the formation pattern with the distance between quadcopters on the X and Y axes in meters. Table IV shows the overall distance in meters as well.

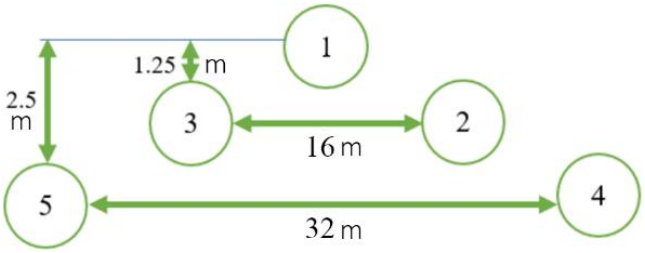


Fig. 4. Illustration of the V-shape formation with distance information

TABLE IV. DISTANCE BETWEEN QUADCOPTERS IN V-SHAPE FORMATION IN METERS

| Q | 1 | 2 | 3 | 4 | 5 |
|---|---|---|---|---|---|
| 1 | 0 | 8.9443 | 8.9443 | 17.89 | 17.89 |
| 2 | 8.9443 | 0 | 16.003 | 8.9443 | 24.331 |
| 3 | 8.9443 | 16.003 | 0 | 24.331 | 8.9443 |
| 4 | 17.89 | 8.9443 | 24.331 | 0 | 32 |
| 5 | 17.89 | 24.331 | 8.9443 | 32 | 0 |

The concept used for the formation control is the distributed guidance route. The leader quadcopter, which is quadcopter 1, provides guidance routes to its two neighboring followers, follower 2 and follower 3 in this case. Then, they will provide another guidance routes to the other two followers, follower 4 and follower 5, respectively. The leader will move to the main target point of the group that has been determined from the beginning. The guiding route provided by the leader is in the form of destination points that changes dynamically based on the leader's position. Define $[x_{target} \;\; y_{target} \;\; z_{target}]^T$ as the $i$-th quadcopter's destination point at each time $t$. The destination point of each follower can be written as follows:

$$X_{target_2}(t) = [x_{leader} + 2l\sin v \;\; y_{leader} - 6l\cos v \;\; z_{leader}] \quad (21)$$

$$X_{target_3}(t) = [x_{leader} - 6l\sin v \;\; y_{leader} + 2l\cos v \;\; z_{leader}] \quad (22)$$

$$X_{target_4}(t) = [x_{follower_2} + 2l\sin v \quad y_{follower_2} - 6l\cos v \quad z_{follower_2}] \tag{23}$$

$$X_{target_5}(t) = [x_{follower_3} - 6l\sin v \quad y_{follower_3} + 2l\cos v \quad z_{follower_3}] \tag{24}$$

Where $l$ is the constant of the formation and $v$ is the angle of the formation. There is also a constant value of 2 and 6 which can be changed according to the desired formation. It can be seen from (21) and (22) that the targets for follower 2 and follower 3 depend on the leader's position. The combination of $x_{target}$ and $y_{target}$ are adjusted so that they are to the right and left of the leader. While $z_{target}$ is equal to the leader's height. Likewise followers 4 and 5, but because they are second-level followers, they get guidance from followers 2 and 3, respectively.

*D. Obstacle Avoidance Control Design*

The Artificial Potential Field (APF) method used is the modified one, namely optimal APF. The algorithm is developed through a scenario where a quadcopter flies in three-dimensional space and its position is $X = (x, y, z)^T$. There are three fields that affect the quadcopter movement. They are an attractive field $U_{att}$ of the target, the repulsive field $U_{rep}$ from obstacles, and the repulsive field from other quadcopters $U_{quad}$ as written here

$$U_{att}(X) = \frac{1}{2}k_{att}\left(X - X_{target}\right)^2 \tag{25}$$

$$U_{rep}(X) = \begin{cases} \frac{1}{2}k_{rep}\left(\frac{1}{\rho(X)} - \frac{1}{\rho_0}\right)^2 \left(X - X_{target}\right)^n, & for\ \rho(X) \le \rho_0 \\ 0, & for\ \rho(X) > \rho_0 \end{cases} \tag{26}$$

$$U_{quad}(i) = \begin{cases} \sum_{j=1}^{m} \frac{1}{2}k_{rep}\left(\frac{1}{\rho(X_{ij})} - \frac{1}{\rho_0}\right)^2 \left(X_i - X_{target}\right)^n, & for\ \rho(X_{ij}) \le \rho_{uav} \\ 0, & for\ \rho(X_{ij}) > \rho_{uav} \end{cases} \tag{27}$$

$k_{att}$ is the attractive gain constant, $X$ is the quadcopter position vector, $X_{target}$ is the target position vector, $k_{rep}$ is the repulsive gain constant, $n$ is any real number whose value is greater than zero, $\rho(X)$ is the distance between the quadcopter's current position and the obstacle, and $\rho_0$ and $\rho_{uav}$ is the influence distant of the repulsive field on the quadcopter from obstacles and other quadcopters, respectively. $\rho(X_{ij})$ is the Euclidean distance between $i$-th quadcopter and $j$-th quadcopter. $m$ is the number of quadcopters.

The three fields will produce their respective forces which produce a resultant force (28) and are explained further by (29) up to (32). $F_{total}$ is the resultant force, $F_{att}$ is the attractive force, $F_{rep}$ is the repulsive force from the obstacle, and $F_{quad}$ is the repulsive force of other quadcopters. The $F_{total}$ has three values, for X, Y, and Z axes. The forces are added to the quadcopter's current position and become reference positions for the flight controller. As for supporting the process of maintaining the formation, the value will be varied if it meets certain criteria. For the leader, if the distance between the leader and one or more of the followers is too far, its forces for the X and Y axes will be divided by 100. On the other hand, if the distance between the follower and its destination is too far, its forces for the X and Y axes will be multiplied by 1.5. That way, on some occasions, the leader will slow down, and the follower will accelerate at the same time. This approach will help the quadcopters to maintain the formation more and smoother trajectory.

One important concept to note is height-based obstacle avoidance. The current APF concept can only do avoidance horizontally. Therefore, the repulsive algorithm will work if $\rho(X) \le \rho_0$ and the height of the quadcopters is 0.075 meters lower than the obstacles ($z - 0.075 \le h_{obstacles}$). A reduction of 0.075 or half of the Quanser Qdrone height in meters is applied because, in real world practice, the height of the quadcopter is calculated from its center of mass which is usually right in the middle of the quadcopter body. In other words, if only ($z \le h_{obstacles}$) is used, the quadcopter body may crash into an obstacle.

$$F_{total}(X) = F_{att}(X) + F_{rep}(X) + F_{quad}(i) \tag{28}$$

$$F_{att}(X) = -grad(U_{att}) = -k_{att}(X - X_{target}) \tag{29}$$

$$F_{rep}(X) = -grad\left(U_{rep}\right) = \begin{cases} F_{rep1}(X) + F_{rep2}(X), & for\ \rho(X) \le \rho_0 \\ 0, & for\ \rho(X) > \rho_0 \end{cases} \tag{30}$$

where

$$F_{rep1}(X) = k_{rep}\left(\frac{1}{\rho(X)} - \frac{1}{\rho_0}\right)\frac{1}{\rho(X)^2}\left(X - X_{target}\right)^n \frac{\partial\rho(X)}{\partial(X)} \tag{31}$$

$$F_{rep2}(X) = -\frac{n}{2}k_{rep}\left(\frac{1}{\rho(X)} - \frac{1}{\rho_0}\right)^2 \left(X - X_{target}\right)^{n-1} \frac{\partial\left(X - X_{target}\right)}{\partial(X)} \tag{32}$$

As explained in the first section, there are two avoidance control strategies that will be compared. First, a strategy where formation is more important than obstacle avoidance. In this strategy, the quadcopters will try to maintain the formation all the time, called total avoidance. Conversely, the second strategy prioritizes obstacle avoidance over formation and is called minimal avoidance. To create both strategies, the evasion radius, $\rho_0$, on APF will be modified.

For total avoidance, the formation will be treated as one body. Therefore, the value of the evasion radius $\rho_0$ is taken from the outermost quadcopter's minimum distance to the obstacle so that the formation will avoid a safe distance for all quadcopters. To achieve this, we use if logic and choose $\rho_0 = 20$ for all conditions. The value 20 is taken because the leader has a distance of about 16 meters from the outermost follower.

As for minimal avoidance, the formation will still be formed and maintained but it can be broken up more easily because the size of the formation is not considered. In some instances, some quadcopters must disengage before returning to formation after avoiding obstacles. Each quadcopter has an evasion radius that varies relative to the size of the obstacle, $\rho_0 = a * radius$. $a$ is a constant whose value can be adjusted and $radius$ is the radius of the obstacles since it is tubular. In this paper, we choose $a = 2$. But the minimal avoidance has a constraint that it only works well when the $radius < \frac{1}{4}$ of the distance between leader and follower 2 or 3. So this strategy will only work if the obstacle has a radius of less than 2, in this case.

Lastly, the combined strategy combines the concepts of total avoidance and minimal avoidance strategy. It is a more versatile strategy based on the faced obstacle.

### E. Formation Performance Index

To see how the performance of the quadcopters maintains the formation, a modified formation performance index is created, which is defined as follows:

$$I(t) = \sum_{i=2}^{5} \left| (\|X_{leader} - X_i\| - \left\|X_{leader} - X_{target_i}\right\| ) \right| \quad (33)$$

Where $I(t)$ is the performance index per unit of time. $X_{leader}$ is the leader position, $X_i$ is the $i$-th follower position, $X_{target_i}$ is the $i$-th follower desired position. The concept of this index is to compare actual formation and formation that should be formed based on the distance of each quadcopter to the leader. The index will be zero if and only if the formation is perfect.

## III. Results and Discussion

The designed algorithm testing will be carried out by combining the two tasks, formation control, and obstacle avoidance, in several scenarios. There are 5 quadcopters moving in formation towards a destination point. The destination point is only known by the leader, while the followers only follow the leader. On the track, there are one or more obstacles that must be avoided. For all tests, the target and initial position of each quadcopter are listed in Table V.

TABLE V. Initial Conditions of Quadcopters and Target

| Parameter | $X(m)$ | $Y(m)$ | $Z(m)$ |
|---|---|---|---|
| Quadcopter 1 | 1 | 1 | 0 |
| Quadcopter 2 | 50 | 1 | 0 |
| Quadcopter 3 | 1 | 50 | 0 |
| Quadcopter 4 | 25 | 20 | 0 |
| Quadcopter 5 | 20 | 25 | 0 |
| Target | 500 | 500 | 30 |

In addition, the value of other parameters is already set. $k_{rep} = 0.04$, $k_{att} = 0.3$, $l = 2$, $v = \frac{\pi}{2}$, $n = 2$, $\rho_0$ of minimal avoidance is $2 * radius$, $\rho_0$ of total avoidance is $\max(2 * radius, 20)$ for obstacles size smaller than 10, and for obstacles bigger than 10, $\rho_0$ of total avoidance is $\min(2 * radius, 20)$. Each case will be tried using total avoidance and minimal avoidance strategies. The value of each gain can change the performance of the entire system. Small values of $k_{att}$ and $k_{rep}$ will make the quadcopter's movements slower but smoother when making a turn. On the other hand, if the values of $k_{att}$ and $k_{rep}$ are too large, the quadcopter movement becomes faster but is very susceptible to excessive movements such as chattering, especially when avoiding obstacles. Meanwhile, $\rho_o$ will determine when avoidance is carried out.

### A. Case I – Big Obstacle Testing

In the first case, the formation will be faced with a large obstacle. This test was conducted to see how large obstacles influence formation behavior. The specification for the obstacle is written in Table VI.

TABLE VI. Obstacle Specification for the First Case

| Obstacle | $X(m)$ | $Y(m)$ | $Z(m)$ | radius |
|---|---|---|---|---|
| Obstacle 1 | 200 | 200 | 50 | 20 |

Fig. 5 shows that the formation with the total avoidance strategy succeeded in carrying out the task. There is no collision between quadcopters or quadcopters that are separated from the formation. Avoidance is carried out at about 20 meters from the outer circle of the obstacle. This distance makes follower 4 quite close to the obstacle, but still at a safe distance. More details are in Fig. 7.

Then from Fig. 6, the result obtained from minimal avoidance is quite similar to total avoidance. However, the formation makes a turn at a greater distance from the obstacle, where twice the radius means about 40 meters from the obstacle. A clearer appearance can be seen in Fig. 8.

Moreover, with the same number of iterations, the total avoidance strategy will reach a farther position than the minimal avoidance. In Fig. 7, the formation has almost reached the destination point which is marked by a red circle. While in Fig. 8, the formation is still in the middle of the road. Of course, a longer turn will result in a longer travel time.

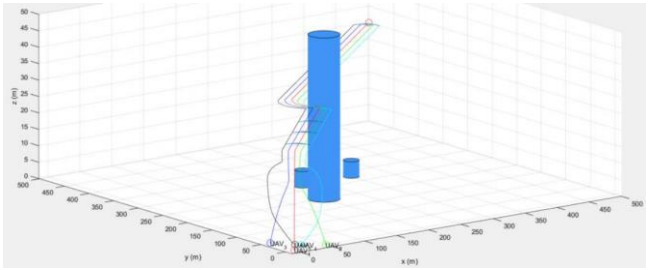

Fig. 5. Test case I – total avoidance

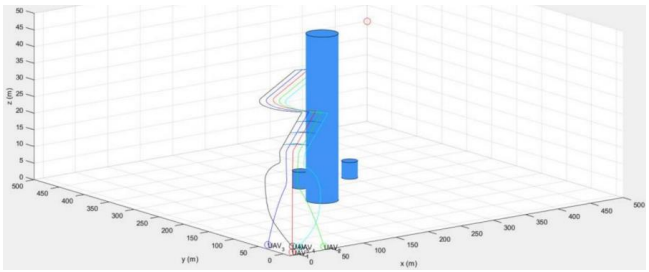

Fig. 6. Test case I – minimal avoidance

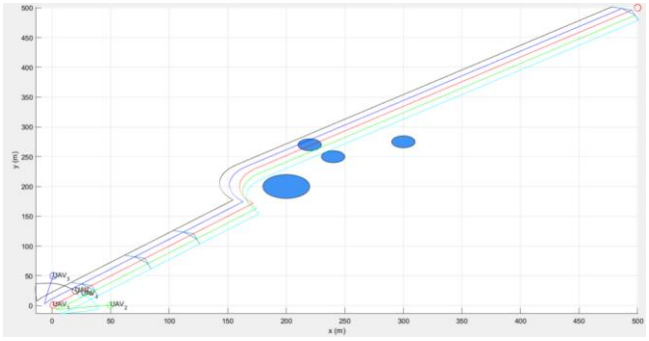

Fig. 7. Top view of case I - total avoidance

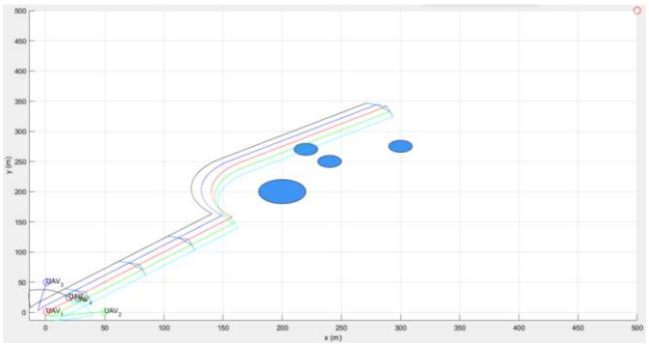

Fig. 8. Top view of case I – minimal avoidance

If we look at Fig. 9, Fig. 10, Fig. 11, there is only a slight deviation in the distance between the leader and its followers. Deviations in the total avoidance strategy occur shorter than the minimal avoidance, none other than because the avoidance distance is longer. After a while, the difference tries to return to its initial value. Uniquely, the shift on the chart is not up but down towards the ideal value of the formation distance. The presence of obstacles makes the movement of the quadcopter slow down so that the desired formation is formed better.

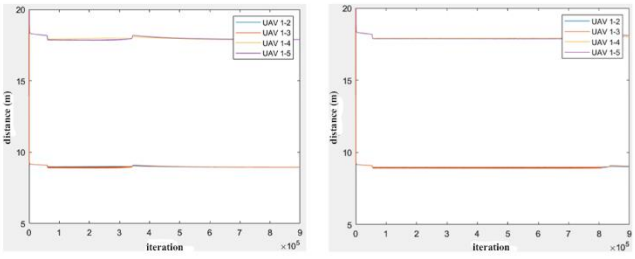


(a) (b)

Fig. 9. The distance between leader and followers in test case I: (a) total avoidance and (b) minimal avoidance

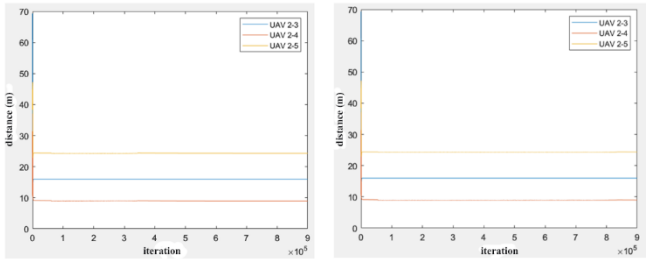


(a) (b)

Fig. 10. The distance between follower 2 and other followers in test case I: (a) total avoidance and (b) minimal avoidance

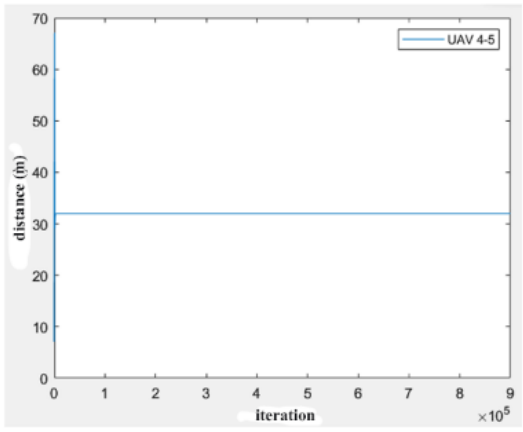


Fig. 11. The distance between follower 4 and follower 5 in test case I: total avoidance and minimal avoidance

Based on Fig. 12, the formation performance index shows good results. Most of the time, the index reaches a fairly low value close to 0, especially when the formation is dodging obstacles. The mean of test case I with total avoidance strategy is 0.2310 while the minimal avoidance is 0.2122.

This whole simulation is completed in about 15 minutes in our computer, corresponding to around 9000 seconds in the real-time metric. This shows that computational complexity may not be a burden on this simulation.

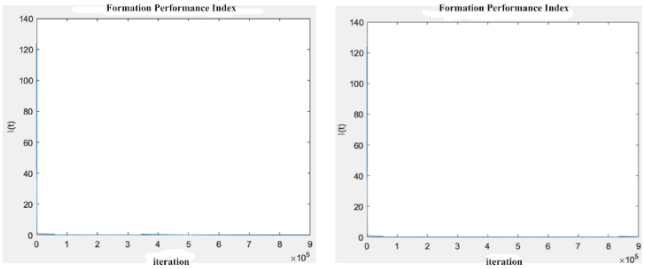


(a) (b)

Fig. 12. Formation performance index for test case I: (a) total avoidance and (b) minimal avoidance

## *B. Case II – Small Obstacle Testing*

Contrary to case I, the obstacle for case II is small enough even smaller than the formation size. The specification of the obstacle is written in Table VII.

TABLE VII. OBSTACLE SPECIFICATION FOR THE SECOND CASE

| Obstacle | $X(m)$ | $Y(m)$ | $Z(m)$ | radius |
|---|---|---|---|---|
| Obstacle 1 | 200 | 200 | 50 | 20 |

For small obstacle avoidance, the total avoidance strategy still provides the same treatment as a large obstacle. The formation remains united because the leader dodges at a distance of about 20 meters, which is safe for the entire formation as shown in Fig. 13 and Fig. 15.

On the other hand, for the minimal avoidance strategy in Fig. 14 and Fig. 16, the formation must be separated to the left and right of the obstacle. The size of the obstacle is small enough so that the gap between quadcopters can pass. Due to the position of the obstacle is right in the middle of the formation route, the leader must evade and deflect the entire formation.

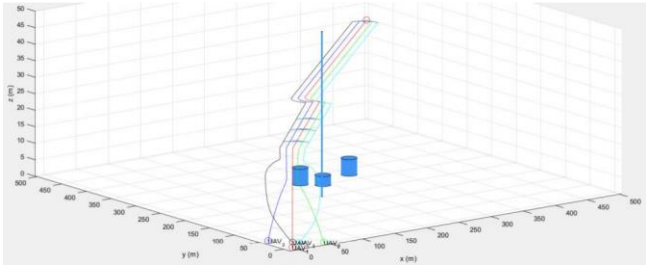

Fig. 13. Test case II – total avoidance

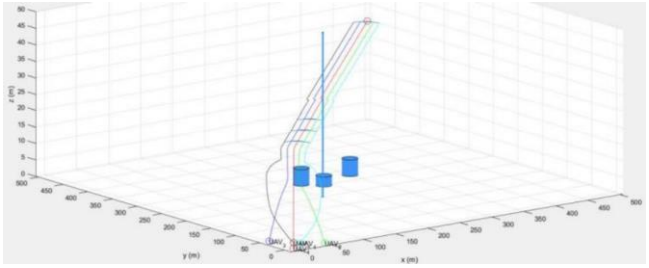

Fig. 14. Test case II – minimal avoidance

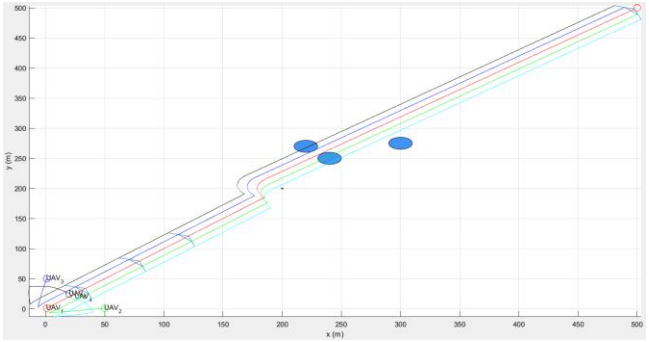

Fig. 15. Top view of case II - total avoidance

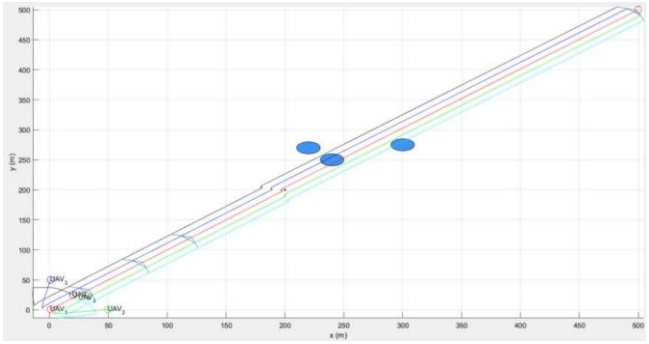

Fig. 16. Top view of case II - minimal avoidance

The same thing happens as in test case 1. In Fig. 17, there is a deviation around iteration 100000 to 200000, or the time when the formation avoids the obstacle. It strengthened the phenomenon that the obstacle perfected the formation. This time, the deviation for minimal avoidance is shorter than total avoidance.

The performance index of test case II also looks good. The average formation performance index for the total avoidance strategy is 0.2164 and for the minimal strategy is 0.2033. The result is shown in Fig. 18.

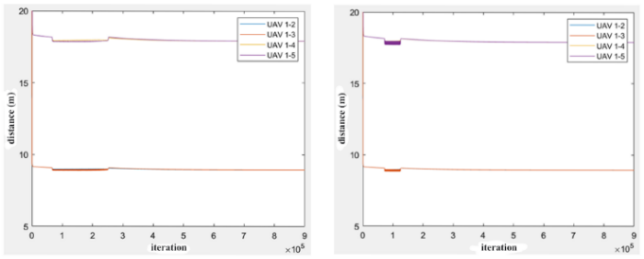

(a) (b)

Fig. 17. The distance between leader and followers in test case II: (a) total avoidance and (b) minimal avoidance

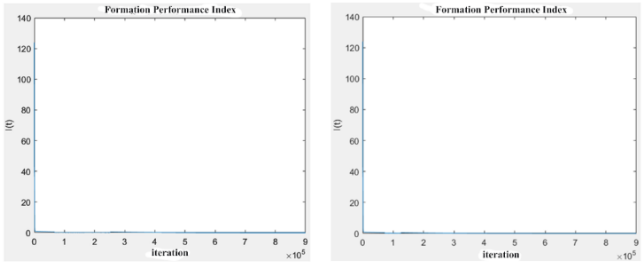

(a) (b)

Fig. 18. Formation performance index for test case II: (a) total avoidance and (b) minimal avoidance

### *C. Case III – Testing with Various Obstacles*

The third case incorporates different forms of obstacles, including variations in height. Obstacle specifications are in Table VIII.

TABLE VIII. OBSTACLE SPECIFICATION FOR THE THIRD CASE

| Obstacle | $X(m)$ | $Y(m)$ | $Z(m)$ | radius |
|---|---|---|---|---|
| Obstacle 1 | 200 | 200 | 50 | 10 |
| Obstacle 2 | 300 | 275 | 50 | 10 |
| Obstacle 3 | 220 | 270 | 5 | 10 |
| Obstacle 4 | 240 | 250 | 30 | 10 |

Fig. 19 represents both total avoidance and minimal avoidance because they have identical results. This phenomenon occurs because the obstacle size, 10, is the value that makes the avoidance radius of both strategies the same so that the resulting behavior is also the same. For total avoidance, the evasion radius is 20. Whereas the minimal avoidance will determine the evasion radius based on 2 times the size of the obstacle, which also happens to be 20 in this case. The formation will avoid the very front obstacle because it is right in the middle and has a height that exceeds the formation's flying height. Then, the formation will also avoid obstacle 4 because its height is as high as the formation. The 0.075 meters rule works in a case like this.

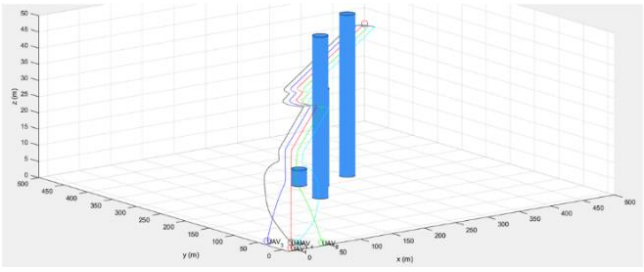

Fig. 19. Test case III – total avoidance and minimal avoidance

As seen in Fig. 20 and Fig. 21, the chart for case III has more ups and downs than the others because the formation needs to do more avoidances along the way. The formation performance index for both strategies has the same average value, which is 0.23.

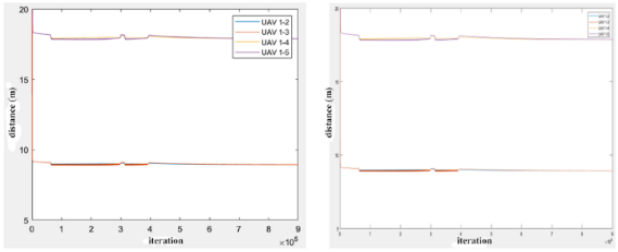


Fig. 20. The distance between leader and followers in test case III: (a) total avoidance and (b) minimal avoidance

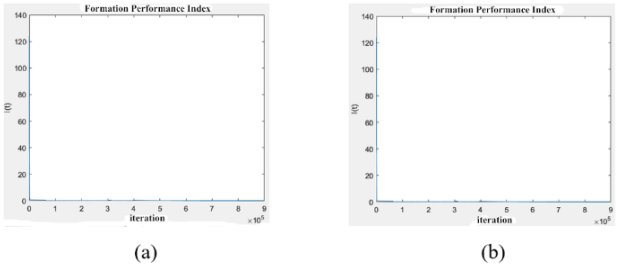


Fig. 21. Formation performance index for test case III: (a) total avoidance and (b) minimal avoidance

### *D. Case IV – Combined Strategy Testing*

For the last case, we use the combined strategy to fly through various obstacles, this time also with variation in radius. The obstacle specifications can be seen in Table IX and the main difference from the rest is the first and second obstacles.

TABLE IX. OBSTACLE SPECIFICATION FOR THE FOURTH CASE

| Obstacle | $X(m)$ | $Y(m)$ | $Z(m)$ | radius |
|---|---|---|---|---|
| Obstacle 1 | 200 | 200 | 50 | 15 |
| Obstacle 2 | 300 | 325 | 50 | 1.5 |
| Obstacle 3 | 220 | 270 | 5 | 10 |
| Obstacle 4 | 240 | 250 | 30 | 10 |

The result is shown in Fig. 22. The formation succeeds in reaching its target by passing three obstacles, two of which are the biggest and the smallest. When facing the biggest obstacle, the formation chooses total avoidance. On the other hand, it chooses minimal avoidance to slip through the smallest obstacle. By selecting the best strategy for a given situation, the movement of the formation becomes more efficient and smoother to achieve the goal.

### *E. Discussion*

In this sub-section, we will discuss some important aspects of the proposed strategies.

The result of the proposed control design is strongly influenced by the selected parameter values. Changing the value of each parameter can change the performance of the entire system as well as the formation. We carried out several experiments using varying gain values, the results of which are shown in Table X. Fig. 23 also shows the first experiment result.

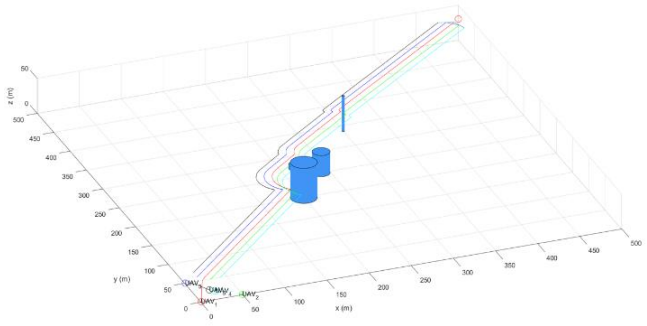


Fig. 22. Test case IV – combined strategy

TABLE X. EFFECT OF APF GAIN VALUES ON SYSTEM PERFORMANCE

| $K_{att}$ | $K_{rep}$ | Result | Total Avoidanc Performance Index | Minimal Avoidance Performance Index |
|---|---|---|---|---|
| 1 | 40 | Very high chattering effect. 2 Quadcopters out of formation during avoidance. | 1.0009 | 4.4143 |
| 1 | 10 | Chattering effect decreased. 2 Quadcopters out of formation | 1.0009 | 1.0009 |
| 1 | 1 | Similar to the previous experiment | 0.9714 | 0.9714 |
| 0.01 | 0.4 | Shows the smoothest results but the slowest movements per iteration. There's still a quadcopter left behind. | 0.8616 | 0.8616 |

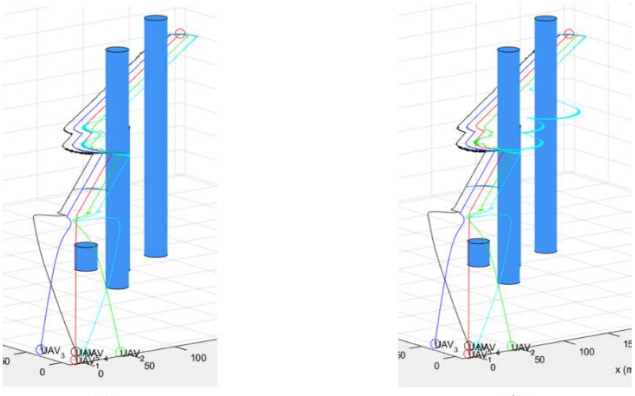


Fig. 23. Simulation with $K_{att}$ = 1 and $K_{rep}$ = 40. (a) Total Avoidance, (b) Minimum Avoidance

These results strengthen the discussion at the beginning of section III regarding the influence of each gain value on system performance.

We have seen how two strategies for obstacle avoidance, total avoidance and minimal avoidance, work in various cases. Experimenting in these diverse environments helps us to see the strengths of each approach. In addition, we never know what kind of obstacles the formation will face on a real

mission so it is good to prepare for as many possible scenarios as possible. The comparisons between them are summarized in Table XI.

TABLE XI. COMPARISON OF TOTAL AND MINIMAL AVOIDANCE

| Criteria | Total Avoidance | Minimal Avoidance |
|---|---|---|
| Path length | Longer for small obstacle | Longer for big obstacle |
| Formation maintenance | More compact | Easier to break |
| Average formation performance index | 0.8000 | 1.2227 |

Then, we will go back to section III.B, where we mentioned that the minimal avoidance strategy only works well with obstacles with $radius < \frac{1}{4}$ of the distance between leader and follower 2 or 3. We believe this statement becomes clearer as we go through the fourth section. In the previous sub-section, the small obstacle has a radius of 1.5 and it goes well. But if we increase the size to 2 for example, follower 3 will be out of formation for a moment of time because the condition is very difficult to deal with. The distance between leader and follower 3 is 8 meters. If the leader, to avoid obstacles, shifts to the left 4 meters, because of $2 * radius$, follower 3 will also shift identically. At that moment, follower 3 will crash into the obstacle as it replaces the leader's previous position. It will try to avoid the obstacle relentlessly and create a kind of chattering movement. So, we put up with the constraint. Of course, the constraint value itself is a variable that changes based on the formation size.

Even though many considerations have been put into the method, of course there are still many possibilities that can be considered for future research, including adaptive methods or dynamic parameter changes. This development can be a bridge for further developments such as different obstacle shapes or different formations.

## IV. CONCLUSION

The use of the guidance route method combined with optimal Artificial Potential Field (APF) is effective for carrying out the task of setting up formations and avoiding obstacles in a group of quadcopters. The average of all formation performance index for the total avoidance strategy is 0.8000 and for the minimal avoidance strategy is 1.2227. These values show that the formation is maintained all the time with only a few errors. Avoidance strategies, both total and minimum avoidance have their own advantages and disadvantages. The total avoidance strategy works better when facing relatively large obstacles. Meanwhile, the minimum avoidance works more efficiently when passing small obstacles. Their use can be adapted to the conditions at hand or perhaps combined to be the combined strategy that implements the advantage of both strategies.

The contribution of this article is the use of optimal APF for quadcopter formation under static obstacles. Several limitations of this work include the limited formation choices as well as the homogeneous agents, which could be considered as the prospect of future research. The future work of this method is to improve the functionality, such as dynamic obstacles, as well as real-world implementation, which may include certain phenomenon such as sensor noise, communication problem, or underactuated systems.

## ACKNOWLEDGMENT

This research was funded by the Department of Electrical Engineering, Institut Teknologi Sepuluh Nopember, Surabaya, Indonesia, with number 1419/PKS/ITS/2023.

## REFERENCES

[1] A. A. Laghari, A. K. Jumani, R. A. Laghari, and H. Nawaz, "Unmanned aerial vehicles: A review," *Cogn. Robot.*, vol. 3, pp. 8–22, 2023, doi: 10.1016/j.cogr.2022.12.004.

[2] N. Islam, M. M. Rashid, F. Pasandideh, B. Ray, S. Moore, and R. Kadel, "A Review of Applications and Communication Technologies for Internet of Things (IoT) and Unmanned Aerial Vehicle (UAV) Based Sustainable Smart Farming," *Sustainability*, vol. 13, no. 4, 2021, doi: 10.3390/su13041821.

[3] A. Mairaj, A. I. Baba, and A. Y. Javaid, "Application specific drone simulators: Recent advances and challenges," *Simul. Model. Pract. Theory*, vol. 94, pp. 100–117, 2019, doi: 10.1016/j.simpat.2019.01.004.

[4] G. E. M. Abro, S. A. B. M. Zulkifli, R. J. Masood, V. S. Asirvadam, and A. Laouiti, "Comprehensive Review of UAV Detection, Security, and Communication Advancements to Prevent Threats," *Drones*, vol. 6, no. 10, 2022, doi: 10.3390/drones6100284.

[5] A. A. Najm and I. K. Ibraheem, "Nonlinear PID controller design for a 6-DOF UAV quadrotor system," *Eng. Sci. Technol. an Int. J.*, vol. 22, no. 4, pp. 1087–1097, 2019, doi: 10.1016/j.jestch.2019.02.005.

[6] E. H. Kadhim and A. T. Abdulsadda, "Mini Drone Linear and Nonlinear Controller System Design and Analyzing," *J. Robot. Control*, vol. 3, no. 2, pp. 212–218, 2022, doi: 10.18196/jrc.v3i2.14180.

[7] S. M. S. Mukras and H. M. Omar, "Development of a 6-DOF Testing Platform for Multirotor Flying Vehicles with Suspended Loads," *Aerospace*, vol. 8, no. 11, 2021, doi: 10.3390/aerospace8110355.

[8] Z. Liu, X. Wang, W. Kang, and Y. Chen, "Research on multi-UAV collaborative electronic countermeasures effectiveness method based on CRITIC weighting and improved gray correlation analysis," *AIP Adv.*, vol. 14, no. 4, p. 45340, Apr. 2024, doi: 10.1063/5.0206440.

[9] K. Guo, X. Li, and L. Xie, "Simultaneous cooperative relative localization and distributed formation control for multiple UAVs," *Sci. China Inf. Sci.*, vol. 63, no. 1, pp. 2019–2021, 2020, doi: 10.1007/s11432-018-9603-y.

[10] M. Sahal, T. Agustinah, A. Jazidie, and H. Du, "Distributed Velocity Control in Cooperative Multi-Agent Moving Source Seeking," *Prz. Elektrotechniczny*, vol. 2023, no. 8, pp. 224–230, 2023, doi: 10.15199/48.2023.08.40.

[11] M. Sahal, T. Agustinah, A. Jazidie, and H. Du, "Strategic Control in Cooperative Multi-Agent Moving Source Seeking with Obstacles Avoidance," *Int. J. Intell. Eng. Syst.*, vol. 16, no. 5, pp. 226–236, 2023, doi: 10.22266/ijies2023.1031.20.

[12] X. Wu, Y. Yin, L. Xu, X. Wu, F. Meng, and R. Zhen, "MULTI-UAV task allocation based on improved genetic algorithm," *IEEE Access*, vol. 9, 2021, doi: 10.1109/ACCESS.2021.3097094.

[13] F. Frattolillo, D. Brunori, and L. Iocchi, "Scalable and Cooperative Deep Reinforcement Learning Approaches for Multi-UAV Systems: A Systematic Review," *Drones*, vol. 7, no. 4, 2023, doi: 10.3390/drones7040236.

[14] Z. Fu, Y. Mao, D. He, J. Yu, and G. Xie, "Secure Multi-UAV Collaborative Task Allocation," *IEEE Access*, vol. 7, 2019, doi: 10.1109/ACCESS.2019.2902221.

[15] S. Li, Y. Jia, F. Yang, Q. Qin, H. Gao, and Y. Zhou, "Collaborative Decision-Making Method for Multi-UAV Based on Multiagent Reinforcement Learning," *IEEE Access*, vol. 10, 2022, doi: 10.1109/ACCESS.2022.3199070.

[16] J. Zhang and J. Xing, "Cooperative task assignment of multi-UAV system," *Chinese J. Aeronaut.*, vol. 33, no. 11, 2020, doi: 10.1016/j.cja.2020.02.009.

[17] Z. Cai, L. Wang, J. Zhao, K. Wu, and Y. Wang, "Virtual target guidance-based distributed model predictive control for formation

control of multiple UAVs," *Chinese J. Aeronaut.*, vol. 33, no. 3, pp. 1037–1056, 2020, doi: 10.1016/j.cja.2019.07.016.

[18] M. A. Kamel, X. Yu, and Y. Zhang, "Formation control and coordination of multiple unmanned ground vehicles in normal and faulty situations: A review," *Annu. Rev. Control*, vol. 49, pp. 128–144, 2020, doi: 10.1016/j.arcontrol.2020.02.001.

[19] B. An, B. Wang, H. Fan, L. Liu, H. Hu, and Y. Wang, "Fully distributed prescribed performance formation control for UAVs with unknown maneuver of leader," *Aerosp. Sci. Technol.*, vol. 130, p. 107886, 2022, doi: 10.1016/j.ast.2022.107886.

[20] T. Yan, Z. Xu, S. X. Yang, and S. A. Gadsden, "Formation control of multiple autonomous underwater vehicles: a review," *Intelligence and Robotics*, vol. 3, no. 1, 2023, doi: 10.20517/ir.2023.01.

[21] Z. S. Lippay and J. B. Hoagg, "Formation Control with Time-Varying Formations, Bounded Controls, and Local Collision Avoidance," *IEEE Trans. Control Syst. Technol.*, vol. 30, no. 1, 2022, doi: 10.1109/TCST.2021.3062824.

[22] H. Liu, T. Ma, F. L. Lewis, and Y. Wan, "Robust Formation Control for Multiple Quadrotors with Nonlinearities and Disturbances," *IEEE Trans. Cybern.*, vol. 50, no. 4, 2020, doi: 10.1109/TCYB.2018.2875559.

[23] Y. Yang, Y. Xiao, and T. Li, "Attacks on Formation Control for Multiagent Systems," *IEEE Trans. Cybern.*, vol. 52, no. 12, 2022, doi: 10.1109/TCYB.2021.3089375.

[24] H. Sheng *et al.*, "New multi-UAV formation keeping method based on improved artificial potential field," *Chinese J. Aeronaut.*, vol. 36, no. 11, pp. 249–270, 2023, doi: 10.1016/j.cja.2023.07.030.

[25] L. Tsiu and E. D. Markus, "A Survey of Formation Control for Multiple Mobile Robotic Systems," *Int. J. Mech. Eng. Robot. Res.*, vol. 9, no. 11, pp. 1515–1520, 2020, doi: 10.18178/ijmerr.9.11.1515-1520.

[26] C. Bai, P. Yan, W. Pan, and J. Guo, "Learning-Based Multi-Robot Formation Control With Obstacle Avoidance," *IEEE Trans. Intell. Transp. Syst.*, vol. 23, no. 8, pp. 11811–11822, 2022, doi: 10.1109/TITS.2021.3107336.

[27] X. Wu, R. Wu, Y. Zhang, and J. Peng, "Distributed Formation Control of Multi-Robot Systems with Path Navigation via Complex Laplacian," *Entropy*, vol. 25, no. 11, 2023, doi: 10.3390/e25111536.

[28] Y. Yang, Y. Xiao, and T. Li, "A Survey of Autonomous Underwater Vehicle Formation: Performance, Formation Control, and Communication Capability," *IEEE Commun. Surv. Tutorials*, vol. 23, no. 2, pp. 815–841, 2021, doi: 10.1109/COMST.2021.3059998.

[29] L. Li, Y. Li, Y. Zhang, G. Xu, J. Zeng, and X. Feng, "Formation Control of Multiple Autonomous Underwater Vehicles under Communication Delay, Packet Discreteness and Dropout," *Journal of Marine Science and Engineering*, vol. 10, no. 7, 2022, doi: 10.3390/jmse10070920.

[30] Q. Zhen, L. Wan, Y. Li, and D. Jiang, "Formation control of a multi-AUVs system based on virtual structure and artificial potential field on SE(3)," *Ocean Eng.*, vol. 253, p. 111148, 2022, doi: 10.1016/j.oceaneng.2022.111148.

[31] B. Andrievsky, A. M. Popov, I. Kostin, and J. Fadeeva, "Modeling and Control of Satellite Formations: A Survey," *Automation*, vol. 3, no. 3, pp. 511–544, 2022, doi: 10.3390/automation3030026.

[32] L. Zhao, C. Yuan, X. Li, and J. He, "Multiple Spacecraft Formation Flying Control around Artificial Equilibrium Point Using Propellantless Approach," *Int. J. Aerosp. Eng.*, vol. 2022, no. 1, p. 8719645, Jan. 2022, doi: 10.1155/2022/8719645.

[33] R. Sun, A. Shan, C. Zhang, and Q. Jia, "Spacecraft formation control using aerodynamic and Lorentz force," *Aircr. Eng. Aerosp. Technol.*, vol. 92, no. 4, pp. 587–597, Jan. 2020, doi: 10.1108/AEAT-10-2019-0207.

[34] T. Wang and J. Huang, "Time-varying formation control with attitude synchronization of multiple rigid body systems," *Int. J. Robust Nonlinear Control*, vol. 32, no. 1, pp. 181–204, Jan. 2022, doi: 10.1002/rnc.5825.

[35] J. Hirata-Acosta, J. Pliego-Jiménez, C. Cruz-Hernádez, and R. Martínez-Clark, "Leader-Follower Formation Control of Wheeled Mobile Robots without Attitude Measurements," *Applied Sciences*, vol. 11, no. 12, 2021, doi: 10.3390/app11125639.

[36] F. Chen and D. V Dimarogonas, "Leader–Follower Formation Control With Prescribed Performance Guarantees," *IEEE Trans. Control Netw. Syst.*, vol. 8, no. 1, pp. 450–461, 2021, doi: 10.1109/TCNS.2020.3029155.

[37] C. Huang, T. Xu, and X. Wu, "Leader–Follower Formation Control of Magnetically Actuated Millirobots for Automatic Navigation," *IEEE/ASME Trans. Mechatronics*, vol. 29, no. 2, pp. 1272–1282, 2024, doi: 10.1109/TMECH.2023.3300010.

[38] X. Chen *et al.*, "A Novel Virtual-Structure Formation Control Design for Mobile Robots with Obstacle Avoidance," *Applied Sciences*, vol. 10, no. 17, 2020, doi: 10.3390/app10175807.

[39] X. Yan, D. Jiang, R. Miao, and Y. Li, "Formation Control and Obstacle Avoidance Algorithm of a Multi-USV System Based on Virtual Structure and Artificial Potential Field," *Journal of Marine Science and Engineering*, vol. 9, no. 2, 2021, doi: 10.3390/jmse9020161.

[40] S. Oh-hara and A. Fujimori, "A Leader-follower formation control of mobile robots by position-based visual servo method using fisheye camera," *ROBOMECH J.*, vol. 10, no. 1, p. 30, 2023, doi: 10.1186/s40648-023-00268-6.

[41] J. Hernandez-Barragan, T. Hernandez, J. D. Rios, M. Perez-Cisneros, and A. Y. Alanis, "Edge-Weighted Consensus-Based Formation Control with Collision Avoidance for Mobile Robots Based on Multi-Strategy Mutation Differential Evolution," *Mathematics*, vol. 11, no. 17, 2023, doi: 10.3390/math11173633.

[42] L. Wang, X. Li, B. Liu, and Z. Zhang, "Consensus Formation Control and Obstacle Avoidance of Multiagent Systems with Directed Topology," *Math. Probl. Eng.*, vol. 2020, no. 1, p. 2637403, Jan. 2020, doi: 10.1155/2020/2637403.

[43] P. Trindade, P. Batista, and R. Cunha, "Third-order consensus for robust distributed formation control of double integrator vehicles," *Control Eng. Pract.*, vol. 133, p. 105436, 2023, doi: 10.1016/j.conengprac.2023.105436.

[44] N. Hacene and B. Mendil, "Behavior-based Autonomous Navigation and Formation Control of Mobile Robots in Unknown Cluttered Dynamic Environments with Dynamic Target Tracking," *Int. J. Autom. Comput.*, vol. 18, no. 5, pp. 766–786, 2021, doi: 10.1007/s11633-020-1264-x.

[45] M. Saska, D. Hert, T. Baca, V. Kratky, and T. Nascimento, "Formation control of unmanned micro aerial vehicles for straitened environments," *Auton. Robots*, vol. 44, no. 6, pp. 991–1008, 2020, doi: 10.1007/s10514-020-09913-0.

[46] G. Khodamipour, S. Khorashadizadeh, and M. Farshad, "Adaptive formation control of leader–follower mobile robots using reinforcement learning and the Fourier series expansion," *ISA Trans.*, vol. 138, pp. 63–73, 2023, doi: 10.1016/j.isatra.2023.03.009.

[47] N. Wang and H. Li, "Leader–follower formation control of surface vehicles: A fixed-time control approach," *ISA Trans.*, vol. 124, pp. 356–364, 2022, doi: 10.1016/j.isatra.2020.05.042.

[48] K. K. Oh, M. C. Park, and H. S. Ahn, "A survey of multi-agent formation control," *Automatica*, vol. 53, pp. 424–440, 2015, doi: 10.1016/j.automatica.2014.10.022.

[49] Q. Chen, Y. Wang, Y. Jin, T. Wang, X. Nie, and T. Yan, "A Survey of An Intelligent Multi-Agent Formation Control," *Applied Sciences*, vol. 13, no. 10, 2023, doi: 10.3390/app13105934.

[50] J. H. Son and M. K. Sung, "Position-Based Formation Control Scheme for Crowds Using Short Range Distance (SRD)," *Applied Sciences*, vol. 14, no. 8, 2024, doi: 10.3390/app14083386.

[51] M. B. Sial *et al.*, "Bearing-Based Distributed Formation Control of Unmanned Aerial Vehicle Swarm by Quaternion-Based Attitude Synchronization in Three-Dimensional Space," *Drones*, vol. 6, no. 9, 2022, doi: 10.3390/drones6090227.

[52] J. Chen, R. Zhou, G. Sun, Q. Li, and N. Zhang, "Distributed formation control of multiple aerial vehicles based on guidance route," *Chinese J. Aeronaut.*, vol. 36, no. 3, pp. 368–381, 2023, doi: 10.1016/j.cja.2022.11.014.

[53] G. Sun *et al.*, "Cooperative formation control of multiple aerial vehicles based on guidance route in a complex task environment," *Chinese J. Aeronaut.*, vol. 33, no. 2, pp. 701–720, 2020, doi: 10.1016/j.cja.2019.08.009.

[54] X. Wang, B. Zerr, H. Thomas, B. Clement, and Z. Xie, "Pattern formation of multi-AUV systems with the optical sensor based on displacement-based formation control," *Int. J. Syst. Sci.*, vol. 51, no. 2, pp. 348–367, Jan. 2020, doi: 10.1080/00207721.2020.1716096.

[55] F. Mehdifar, C. P. Bechlioulis, F. Hashemzadeh, and M. Baradarannia, "Prescribed performance distance-based formation control of Multi-Agent Systems," *Automatica*, vol. 119, p. 109086, 2020, doi: 10.1016/j.automatica.2020.109086.

[56] N. Wang, J. Dai, and J. Ying, "UAV Formation Obstacle Avoidance Control Algorithm Based on Improved Artificial Potential Field and Consensus," *Int. J. Aeronaut. Sp. Sci.*, vol. 22, no. 6, pp. 1413–1427, 2021, doi: 10.1007/s42405-021-00407-6.

[57] Y. Liu, J. Zhang, Y. Zhang, and J. Wang, "Virtual Streamline Traction: Formation Cooperative Obstacle Avoidance Based on Dynamical Systems," *Applied Sciences*, vol. 14, no. 14, 2024, doi: 10.3390/app14146087.

[58] J. Guo, C. Liang, K. Wang, B. Sang, and Y. Wu, "Three-Dimensional Autonomous Obstacle Avoidance Algorithm for UAV Based on Circular Arc Trajectory," *Int. J. Aerosp. Eng.*, vol. 2021, no. 1, p. 8819618, Jan. 2021, doi: 10.1155/2021/8819618.

[59] Y. Wu, J. Gou, X. Hu, and Y. Huang, "A new consensus theory-based method for formation control and obstacle avoidance of UAVs," *Aerosp. Sci. Technol.*, vol. 107, p. 106332, 2020, doi: 10.1016/j.ast.2020.106332.

[60] L. Ji, X. Qu, C. Tang, S. Yang, X. Guo, and H. Li, "Consensus Formation of Multi-agent Systems with Obstacle Avoidance based on Event-triggered Impulsive Control," *J. Intell. Robot. Syst.*, vol. 109, no. 3, p. 61, 2023, doi: 10.1007/s10846-023-01987-z.

[61] B. Wei, "UAV formation obstacle avoidance control method based on artificial potential field and consistency," *J. Phys. Conf. Ser.*, vol. 2083, no. 4, p. 42029, 2021, doi: 10.1088/1742-6596/2083/4/042029.

[62] H. Huang, W. Ma, J. Li, and Y. Fang, "Intelligent obstacle avoidance control method for unmanned aerial vehicle formations in unknown environments," *J. Tsinghua Univ. (Science Technol.*, vol. 64, no. 2, pp. 358–369, 2024, doi: 10.16511/j.cnki.qhdxxb.2023.27.001.

[63] B. Sharma, M. S. Obaidat, V. Sharma, and K.-F. Hsiao, "Routing and collision avoidance techniques for unmanned aerial vehicles: Analysis, optimal solutions, and future directions," *Int. J. Commun. Syst.*, vol. 33, no. 18, p. e4628, Dec. 2020, doi: 10.1002/dac.4628.

[64] T. Zhang and X. Zhang, "Distributed Model Predictive Control with Particle Swarm Optimizer for Collision-Free Trajectory Tracking of MWMR Formation," *Actuators*, vol. 12, no. 3, 2023, doi: 10.3390/act12030127.

[65] W. Yu and Y. Lu, "UAV 3D environment obstacle avoidance trajectory planning based on improved artificial potential field method," *J. Phys. Conf. Ser.*, vol. 1885, no. 2, 2021, doi: 10.1088/1742-6596/1885/2/022020.

[66] Y. Ning, M. Yue, L. Guo, and J. Zhao, "A wip vehicle control method based on improved artificial potential field subject to multi-obstacle environment," *Inf. Technol. Control*, vol. 49, no. 3, 2020, doi: 10.5755/j01.itc.49.3.25477.

[67] J. Tang, J. Sun, C. Lu, and S. Lao, "Optimized artificial potential field algorithm to multi-unmanned aerial vehicle coordinated trajectory planning and collision avoidance in three-dimensional environment," *Proc. Inst. Mech. Eng. Part G J. Aerosp. Eng.*, vol. 233, no. 16, 2019, doi: 10.1177/0954410019844434.

[68] Z. Pan, C. Zhang, Y. Xia, H. Xiong, and X. Shao, "An Improved Artificial Potential Field Method for Path Planning and Formation Control of the Multi-UAV Systems," *IEEE Trans. Circuits Syst. II Express Briefs*, vol. 69, no. 3, 2022, doi: 10.1109/TCSII.2021.3112787.

[69] H. Song, S. Hu, W. Jiang, Q. Guo, and M. Zhu, "Artificial Potential Field-Based Multi-UAV Formation Control and Target Tracking," *Int. J. Aerosp. Eng.*, vol. 2022, 2022, doi: 10.1155/2022/4253558.

[70] T. Xing, X. Wang, K. Ding, K. Ni, and Q. Zhou, "Improved Artificial Potential Field Algorithm Assisted by Multisource Data for AUV Path Planning," *Sensors*, vol. 23, no. 15, 2023, doi: 10.3390/s23156680.

[71] G. Hao, Q. Lv, Z. Huang, H. Zhao, and W. Chen, "UAV Path Planning Based on Improved Artificial Potential Field Method," *Aerospace*, vol. 10, no. 6, 2023, doi: 10.3390/aerospace10060562.

[72] J. Li, Y. Fang, H. Cheng, Z. Wang, and S. Huangfu, "Unmanned aerial vehicle formation obstacle avoidance control based on light transmission model and improved artificial potential field," *Trans. Inst. Meas. Control*, vol. 44, no. 16, pp. 3229–3242, Jun. 2022, doi: 10.1177/01423312221100340.

[73] P. Yang, Y. Xuan, and W. Li, "Adaptive Nonsingular Fast-Reaching Terminal Sliding Mode Control Based on Observer for Aerial Robots," *Actuators*, vol. 13, no. 3, 2024, doi: 10.3390/act13030098.

[74] X. Zhang *et al.*, "Finite-Time Adaptive Quantized Control for Quadrotor Aerial Vehicle with Full States Constraints and Validation on QDrone Experimental Platform," *Drones*, vol. 8, no. 6, 2024, doi: 10.3390/drones8060264.

[75] P. K. Muthusamy *et al.*, "Self-Organizing BFBEL Control System for a UAV Under Wind Disturbance," *IEEE Trans. Ind. Electron.*, vol. 71, no. 5, pp. 5021–5033, 2024, doi: 10.1109/TIE.2023.3285922.

[76] C. Li, Y. Wang, and X. Yang, "Adaptive fuzzy control of a quadrotor using disturbance observer," *Aerosp. Sci. Technol.*, vol. 128, p. 107784, 2022, doi: 10.1016/j.ast.2022.107784.

[77] B. Wang, Y. Zhang, and W. Zhang, "Integrated path planning and trajectory tracking control for quadrotor UAVs with obstacle avoidance in the presence of environmental and systematic uncertainties: Theory and experiment," *Aerosp. Sci. Technol.*, vol. 120, p. 107277, 2022, doi: 10.1016/j.ast.2021.107277.

[78] J. W. Lee, N. Xuan-Mung, N. P. Nguyen, and S. K. Hong, "Adaptive altitude flight control of quadcopter under ground effect and time-varying load: theory and experiments," *JVC/Journal Vib. Control*, vol. 29, no. 3–4, 2023, doi: 10.1177/10775463211050169.

[79] G. P. Rible, N. A. Arriola, and M. Ramos, "Modeling and implementation of quadcopter autonomous flight based on alternative methods to determine propeller parameters," *Adv. Sci. Technol. Eng. Syst.*, vol. 5, no. 5, 2020, doi: 10.25046/AJ050589.

[80] C. A. I. Zhenhuan, S. Zhang, and X. Jing, "Model predictive controller for quadcopter trajectory tracking based on feedback linearization," *IEEE Access*, vol. 9, 2021, doi: 10.1109/ACCESS.2021.3134009.

[81] S. Nurjanah, T. Agustinah, and M. Fuad, "Cooperative Position-based Formation-pursuit of Moving Targets by Multi-UAVs with Collision Avoidance," *AREE (Journal on Advanced Research in Electrical Engineering)*, vol. 6, no. 2, pp. 82–90, 2022.

[82] Quanser, "QDrone Product Data Sheet v1.3," 2018, https://www.quanser.com/wp-content/uploads/2018/02/QDrone-Product-Data-Sheet-v1.3.pdf.